

INTERIM REPORT

Optimal Sensor Management and Signal Processing for
New EMI Systems

SERDP Project MR-1708

SEPTEMBER 2010

Lawrence Carin
Nilanjan Dasgupta
Levi Kennedy
Signal Innovations Group, Inc.

This document has been approved for public release



This report was prepared under contract to the Department of Defense Strategic Environmental Research and Development Program (SERDP). The publication of this report does not indicate endorsement by the Department of Defense, nor should the contents be construed as reflecting the official policy or position of the Department of Defense. Reference herein to any specific commercial product, process, or service by trade name, trademark, manufacturer, or otherwise, does not necessarily constitute or imply its endorsement, recommendation, or favoring by the Department of Defense.

I. ABSTRACT

This document serves as the Interim Report on the project titled “Optimal Sensor Management for Next-Generation EMI Systems” (MM-1708). A significant problem with next-generation EMI systems is the time required to collect all data, and this limitation often necessitates *a priori* hardware compromises that undermine subsequent system performance. SIG had proposed adaptive approaches that would allow one to retain full EMI hardware functionality, while jointly optimizing the accuracy of the extracted geophysical parameters of buried anomalies and the use of available resources (data collection time and battery power). SIG has developed an adaptive sensor-management architecture for next-generation EMI systems, while also being applicable for optimal deployment of existing man-portable (hand-held) systems. We have successfully implemented this framework on the TEMTADS and MetalMapper sensor systems, two of the next-generation multi-axis multi-sensor systems that produced superior UXO discrimination performance during the recently conducted SLO demonstration study. Our analysis shows that by actively selecting the sequence of transmitters and receivers for data collection, one could extract model parameters of buried anomalies using only a fraction of the available Tx-Rx combinations, and thereby saving data collection time and energy resources. The developed framework has also been tested on simulated hand-held equivalent of a TEMTADS system, enabling us to compare the performance of a handheld system with respect to the towed-array system. Similar analysis on MetalMapper data shows that one may use only a subset of the available receivers to obtain accurate inversion of geophysical parameters, thereby suggesting a compact hardware design for the MetalMapper system in future without sacrificing the quality of collected data.

II. OBJECTIVE

The main objective of the project is to develop adaptive algorithms that will allow hardware designers to keep the full functional capability of a next-generation EMI system, while optimally utilizing the available sensors to detect and discriminate buried UXO with minimal sensing actions. The current program seeks to address the following question: Can we design an adaptive sensing strategy that will guide the sensor system on the ground to make a sequence of sensing actions in order to optimally detect and classify a buried object. Recent demonstration at Camp San Luis Obispo (SLO) suggests that next-generation sensor systems like TEMTADS and MetalMapper can successfully detect all buried UXO and successfully classify most of them with low false alarm rate. Both TEMTADS and MetalMapper system were deployed in cued mode, in which potential anomaly locations have been detected by another sensor (EM61). The task of these sensors were to move to each of these locations and make a series of measurements. Rather than activating all Tx-Rx combinations in a predefined sequence to collect data and extract the underlying model parameters offline, SIG proposed a joint data collection and feature extraction approach that adaptively identifies a sequence of the Tx-Rx pairs to activate, with an objective of reliably extracting model parameters with minimal sensing actions.

SIG has developed two adaptive techniques that would improve the speed of data collection and increase the mobility of a TEMTADS system. Although an active learning technique would ideally be incorporated within the sensor system to guide ground personnel on where (location) and how (sensor configuration) to collect data, SIG has simulated the active selection based on the data already collected at Camp SLO. In this setup, the active learning approach was constrained to work only on a 5x5 grid (corresponding to twenty five transmitters and co-located receivers). The first technique assumes that active learning will

identify which of the twenty-five transmitters needs to be activated at any time, while collecting response on all twenty-five receivers. Results show that adaptive sensor scheduling will accurately and reliably estimate the geophysical parameters of a buried anomaly with less number of transmitter firings than a pre-assigned Tx-Rx combinations, improving both the speed of data collection and resource (battery) utilization. In the second approach, SIG has developed an active sensing framework for a hand-held TEMTADS systems (simulated from already available data on a 5x5 grid). This approach adaptively identifies a sequence of sensing location that would provide performance similar to the currently deployed towed-array system. The objective of this approach is to analyze whether a handheld TEMTADS system guided adaptively on a 5x5 grid can provide high quality data suitable for reliable model parameter extraction with minimal number of sensing actions.

MetalMapper system has performed superior to most of the other deployed sensors in discriminating UXO from clutter during the recently conducted UXO discrimination study at camp San Luis Obispo (SLO). In addition to the TEMTADS-based adaptive sensing techniques, SIG has also incorporated the active selection framework for the MetalMapper system, with an objective of identifying optimal subset of transmitter-receiver combinations that obtains reliable extraction of anomaly features. Our analysis shows that one may use only a small fraction of available sensing modes to obtain reliable parameter estimates, and suggests that a more compact, easy-to-maneuver MetalMapper system will be equally effective in UXO detection and classification.

III. TECHNICAL SECTION

The technology developed for adaptive sensing will be described in this section, followed by performance evaluation and conclusions. In this section, we shall first present a background of the work, followed by a brief description of the active learning algorithm. Details of the algorithm can be found in [1]. A brief description of the TEMTADS and MetalMapper system are also presented here for completeness. More information can be obtained from the demonstration reports submitted to the ESTCP program office by the respective developers (SAIC for TEMTADS and Snyder Geoscience for MetalMapper).

A. Background

The detection and remediation of unexploded ordnance (UXO) remains a high priority for the Department of Defense (DoD). According to the Defense Science Board report (2003) [2], the UXO cleanup problem is massive in scale, involving more than ten million acres of land in United States alone. The cost of cleanup consists of detection and excavation of UXO. The problem is aggravated by the fact that most of the state-of-the-art sensor systems have high false alarm rate due to the presence of geological and cultural clutter. Therefore, a significant focus has been directed towards developing improved sensor systems and improved statistical inference techniques that utilize such sensor data to significantly minimize the false alarms, and thereby drastically reduce cleanup costs.

Multi-coil electromagnetic induction (EMI) sensors have performed well on detection and characterization of buried UXO [3], as they are capable of identifying target shape parameters (measured in terms of magnetic polarizabilities), in addition to target depth and orientation. SERDP and ESTCP have funded the design and testing of several multi-coil EMI systems, such as TEMTADS, MetalMapper and BUD (Berkeley UXO Discriminator) that provide significant capability and diversity with respect to the shape

of the incident magnetic field, as well as in how the induced magnetic fields are measured (*e.g.*, multi-field-component measurements).

The large number of sensor parameters (number of transmit/receive coils, number of time gates, etc) often necessitate hardware design tradeoffs, with the goal of achieving practical sensing costs (*e.g.*, sensing time and power consumption). By making these sensor-design tradeoffs in hardware, one necessarily loses functionality, limiting the utility of the system (*e.g.*, the system may have to be tailored in hardware to particular classes of UXO, and UXO depths). SIG had developed an *adaptive* EMI-sensing framework for next-generation EMI systems under SERDP-SEED MM1591 which produced promising results on simulated data. The objective of current work was to bring our algorithmic approach, demonstrated successfully in the SEED project, a step closer to transitioning or deployment for UXO actual remediation by continually testing and validating the sensing models based on the measured data from Camp SLO, as well as other available data. The PI's longstanding relationship with the sensor developers (SAIC and Skip Snyder of Snyder Geoscience) were leveraged to ensure that model development and validation are properly synchronized.

B. Active Learning for Model Parameter Inference

The objective of active learning is to efficiently estimate the parameters of a buried UXO using as few sensing actions as possible. This approach is applicable to the parameters of *any* target model, and therefore it is of utility as models improve under separate SERDP support. It is important to emphasize that this adaptive sensor-optimization algorithm requires *no* training data, and therefore we do not need to know what type of UXO and clutter are present on a given site. The unique aspect of the proposed research is that here information-based active learning is proposed to optimally deploy the sensor for data acquisition (not to define labeled data).

Recent studies have shown that fitting EMI data to a dipole model lead to an efficient estimate of the model parameters, that often may be reliably used in subsequent classification strategies. A buried metallic object, modeled as a single dipole, is fully characterized by the following parameters Θ [4]:

- Relative location of the dipole (x,y,z) with respect to the sensor
- Strength or dipole moment $(M_x, M_y$ and $M_z)$. Note that in practice (*e.g.*, in the Sibert study), we obtained best results when M_x and M_y are assumed to be equal.
- Orientation of the dipole (azimuth θ , and inclination ϕ)
- Resonant frequencies $(w_x, w_y$ and $w_z)$.

We developed an optimal sequential search strategy to infer target parameters $\Theta=(x,y,z,M_x,M_z,w_x,w_z)$. This approach develops a fundamental information-theoretic framework to adaptively and sequentially identify sensing locations in order to minimize the uncertainty on the target-parameter estimation. We also emphasize that this framework is applicable to any sensor type (EMI and magnetometer, and even acoustic), hand-held or cart-based systems, and any class of target models.

Suppose all prior knowledge about the UXO site is described in terms of a prior distribution on the model parameters $p(\Theta)$. Let p_n be the sensor parameters (location and orientation for both transmitter and receiver coils), and O_n be the time-domain sensing data with the n^{th} measurement (sensing action). The algorithm seeks to answer the following question: Where (location) and how (sensor configuration) should the next sensing action be performed (*i.e.*, how to choose p_{n+1}) such that the model parameters could be ascertained with minimal cost (*e.g.*, sensing cost, resource cost on exciting the transmitter coils,

and cost of moving between successive sensing locations). We propose a greedy search strategy where a new sensing location and/or configuration is chosen at every step, based on all prior sensing actions and observations.

The search strategy assumes that the N^{th} measurement is represented as $O_N(p_N, \Theta) = B_{total}(\Theta, p_N) + G_N$, where $B_{total}(\Theta, p_N)$ is the noise-free dipole response, and G_N is additive white Gaussian noise representing a collection of sensor noise and noise/error from geological clutter. The search strategy is based on choosing the sensor parameter p_{N+1} (the next search location and sensor configuration) that minimizes the uncertainty in the model parameter estimates, quantified in terms of Cramer-Rao bound (CRB) [5] and computed as the variance of the unbiased estimate of Θ_{N+1} . Assuming white Gaussian noise, the maximum-likelihood estimation [6] of sensor parameters Θ , based on N sequential measurements $\{p_n, O_n\}_{n=1:N}$, reduces to a least-square (LS) fit [5]

$$\hat{\Theta} = \arg \min_{\Theta} \sum_{n=1}^N |B_{total}(\Theta, p_n) - O_n(p_n)|^2, \quad (1)$$

where $\Theta = [x, y, z, \theta, \phi, M_x, w_x, M_z, w_z]$ represent the target parameters, and p_N represents the sensor parameters (location and configuration). Assuming the underlying noise is white Gaussian, the quality of the estimate of the model parameters, given a sequence of N sensing {actions, observation} tuple $\{p_n, O_n\}_{n=1}^N$ is given by the Fisher Information matrix [7]

$$J = \beta \sum_{n=1}^N \text{Re}\{[\nabla_{\Theta} B_{total}(\Theta, p_n)][\nabla_{\Theta} B_{total}(\Theta, p_n)]^H\}, \quad (2)$$

where ∇_{Θ} represents the gradient evaluated with respect to the target parameters Θ , and superscript H represents the complex transpose. The above equation is evaluated at $\Theta = \hat{\Theta}_N$ (*i.e.*, target parameter estimate based on N observations), assuming the model parameter estimate is correct after N measurements. The objective in selecting the next sensor parameters p_{N+1} is to reduce the uncertainty in the estimated target parameters, characterized through the Cramer-Rao bound $C_B = J^{-1}$ [8]. The uncertainty is quantified in terms of the Fisher information measure q of a measurement sequence $\{p_n, O_n\}_{n=1}^N$ as

$$q(\{p_1, p_2, \dots, p_N\}) = |J(p_1, p_2, \dots, p_N)| = \left| \sum_{n=1}^N J^n(p_n) \right|, \quad (3)$$

Assuming that a new sensor location p_{N+1} is chosen for the subsequent $N + 1^{th}$ measurement, the cumulative Fisher information measure for all measurements *including* the latest measurement is given by

$$\begin{aligned} q(\{p_1, p_2, \dots, p_{N+1}\}) &= \left| \sum_{n=1}^N J^n(p_n) + \beta F(p_{N+1}) F^T(p_{N+1}) \right|, \\ &= \left| \sum_{n=1}^N J^n(p_n) \right| \left| I + \beta F^T \left(\sum_{n=1}^N J^n(p_n) \right)^{-1} F \right|, \end{aligned} \quad (4)$$

where I is a 2×2 identity matrix, and $F = \nabla_{\Theta} B_{total}(\Theta, p_n)$. The logarithmic increase of the Fisher information measure is given by

$$\delta(p) = \ln q(\{p_1, p_2, \dots, p_{N+1}\}) - \ln q(\{p_1, p_2, \dots, p_N\}) = \ln |I + \beta F^T B_N^{-1} F|, \quad (5)$$

where $B_N = \sum_{n=1}^N J^n$ is the Fisher information matrix computed using the first N sensor parameters $\{p_n\}_{n=1}^N$, based on the latest estimate of the model parameters $\hat{\Theta}_N$. Therefore, the sensor parameters p_{N+1} for the $N + 1^{th}$ measurement are selected at a location where the model “error bars” are largest. Since our objective is to achieve the maximum information gain (or maximum reduction in parameter uncertainties), we define the optimal sensing location p_{N+1} as

$$p_{N+1} = \arg \max_p \delta(p) = \arg \max_p \ln |I + \beta F^T B_N^{-1} F| \quad (6)$$

The target parameter estimate is updated ($\hat{\Theta}_N$) based on $\{p_n, O_n\}_{n=1}^{N+1}$. This sequential process of choosing sensor locations/configuration for measurements is terminated when the Fisher information gain is below an user-defined risk criteria, yielding a stable estimate of the approximate UXO location, orientation and other geophysical parameters. The risk criterion need to be chosen carefully based on maximum allowable risk for mislabeling a buried anomaly. The main objective of active learning is to estimate the anomaly parameters with as few sensing actions as possible and thereby avoid excavation of a large number of benign clutter. Active learning identifies the model parameters which are subjected to a classifier that infers a label for the buried anomaly. Higher error in estimating the true model parameters lead to higher level of error in classifying these objects. Since we have solely focused on active learning of anomaly parameters in this research, we decided to stop active learning when the estimated model parameters have stabilized (*i.e.*, the estimated model parameters do not change after a new sensing action is taken).

C. TEMTADS System

A collaboration of researchers from SAIC and NRL have developed a next-generation multi-coil sensor system in a vehicle-towed configuration [9]. The Time Domain Electromagnetic Towed Array Detection System (TEMTADS) is an ultra-wideband EMI sensor system with novel waveforms and multi-axis or vector receivers, consisting of twenty five transmitters and co-located receivers, arranged in a 5x5 grid (see Fig. 1). Each of the bigger squares (numbered from 0 to 24 in the figure) represents a transmitter coil and a smaller concentric square represents a receiver coil. During the SLO data collection, the TEMTADS system was deployed in cued mode. An EM61 sensor surveyed the entire area to identify potential anomaly locations and TEMTADS was used to take measurement at those locations. Once the system is towed and placed over a buried anomaly, the sensor activated all twenty five transmitter loops in a *pre defined* sequence, and for each transmitter firing all receivers were used to collect data, measuring the complete transient response over a wide dynamic time range going approximately from 42 μ sec to 25 msec and distributed in 115 time gates. Thus, a TEMTADS collection at any anomaly location provided 625 time-domain responses, without the need for a relative positioning system due to its fixed geometry.

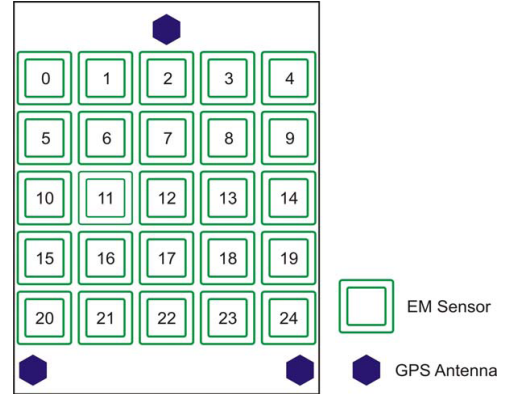


Fig. 1. Configuration of a TEMTADS system

D. MetalMapper System

MetalMapper is a multisensor TEM and Magnetic Gradiometer system for UXO Detection and Classification, developed by Geometrics, Inc. The system has dual-mode (EM/MAG) capability and three orthogonal transmitter loops in the shape of 1m square. The platform includes a spatial array of seven three-axis receiver antennas (as shown in Fig. 2(b)) in the horizontal plane, resulting in 21 independent



Fig. 2. (a) MetalMapper system being towed by a tractor, (b) Schematic of a MetalMapper sensor array, where three mutually orthogonal squares represent three transmitters and blue cubes in the horizontal plane represent the multi-axis receiver arrays.

measurements of the secondary magnetic field corresponding to each of the three transmitters (T_x, T_y and T_z). MetalMapper was deployed in both survey and cued mode during the SLO study. First, the system was deployed in the survey mode identifying anomaly locations that are above an user-defined threshold. Subsequently, the system is placed directly above each “detection” and a set of twenty-one observations were collected. The extraction of features and subsequent classification of the buried anomalies were performed off-line during the SLO demonstration study.

IV. PERFORMANCE ANALYSIS

SIG has demonstrated the efficacy of an adaptive sensing approach in the SEED program (SERDP-SEED-1591) using simulated data. As indicated above, validation and refinement of the adaptive sensor-management techniques to real field data is an important component of the current program, thereby enhancing the utility of the algorithms, and increasing the likelihood of transitions to the field. As mentioned in our proposal, SIG had proposed four principal tasks under the current research program. The first task constituted the development of an active-learning based adaptive sensing technique for optimal deployment of a sensor to estimate the model parameters (features) of a buried anomaly. The proposed duration of this task was one year ending in July 2010. SIG is performing on schedule to complete this task within the proposed time frame. We are simultaneously working on task 4, which includes testing and validation of the active-learning algorithm on data collected at SLO.

The objective of an active learning scheme is to guide the user to make as few sensing actions as possible to reliably estimate the location and geophysical parameters of the buried UXO. As mentioned above, TEMTADS system was deployed in cued mode during the SLO demonstration study, where data collection and feature extraction were done separately. Towing a big and bulky TEMTADS system was slow and it was difficult to position exactly above a detected anomaly in a challenging terrain. The towed-array system that was deployed in SLO demonstration study was capable of covering only 125-140 anomalies per day. In order to alleviate the challenges posed by slow collection of data and slow movement between anomaly locations, SIG has developed two adaptive learning approaches for model parameter inversion. In the first approach, we assume that one of the twenty-five transmitters would be activated at any time,

and anomaly response would be recorded at all receivers. Ideally, one would like to execute the active learning algorithm in real-time, where at each instance, a transmitter is fired from a chosen location. We have simulated this scenario by allowing only twenty-five transmitters and receivers locations for which we already possess data. The corresponding response will be analyzed, and the next “best” action will be identified, *i.e.*, which transmitter needs to be fired next. The next “best” action is chosen in order to maximally reduce the uncertainty in the model parameters of the underlying anomaly. Rather than using a fixed sequence, transmitters would be chosen adaptively using an information-theoretic approach.

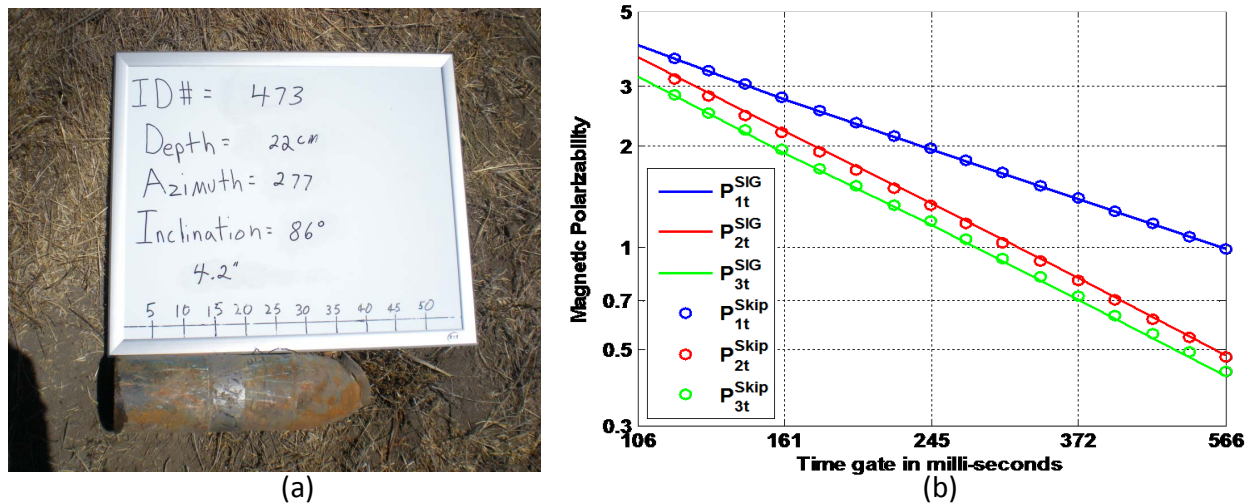


Fig. 3. (a) This image shows a 4.2inch mortar (ID:473) after it has been excavated from the ground, (b) This plot shows the variation of the extracted magnetic polarizabilities along three principal directions as a function of response time. We obtain a strong magnetic moment (in blue) and two other near-similar moments (in red and green), as expected from a axissymmetric cylindrical 4.2inch mortar. Note that the circles represent the moments extracted by Skip Snyder of Snyder Geoscience, whereas the feature extracted by SIG is shown as lines.

Figure 3(a) shows the image of a 4.2inch mortar (ID:337) after it has been excavated from the ground. The figure on the right shows the variation of the extracted features (three principal magnetic polarizabilities) as a function of the response time. The TEMTADS system collects responses over 115 timegates spread between $42\mu\text{sec}$ and 25msec . However, SIG chose five logarithmically spaced timegates to perform feature extraction to obtain fast convergence of the inversion algorithm. The plot also shows that the features extracted by Skip Snyder of Snyder Geoscience (plotted as blue, red and green circles) are almost identical to the SIG-extracted features. Note that the feature extraction shown above utilized data from all twenty-five transmitter-receiver combinations. For all subsequent analysis, SIG will use the features extracted using all available data as the ground truth to compare the performance of the active-learning based adaptive sensing approach with respect to the fixed/non-adaptive sampling.

Figure 4 compares the performance of the adaptive sensing with pre-decided sequential sampling. Figure 4(a) displays the sequential choice of the transmitters as indexed by the number in red. Note that the sequence is fixed and pre-decided, independent of the location of the anomaly. The background shows the monostatic response of the anomaly as received by the twenty five receivers at the first time gate. For better visualization, we have interpolated the response collected over a 5×5 grid to produce a smooth image. Figure 4(b) compares the performance of the adaptive sensing scheme with the uniform sampling, where

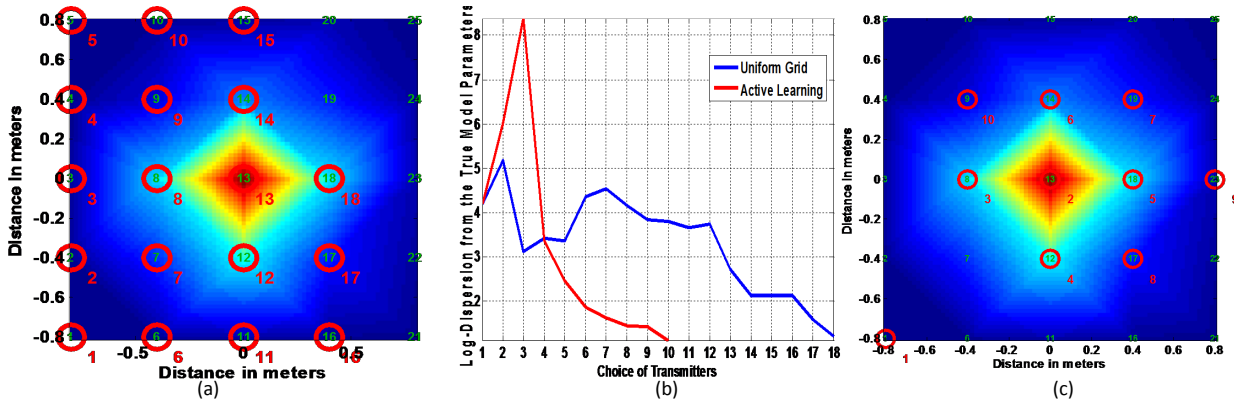


Fig. 4. (a) This plot shows the sequential choice transmitter’s activations for uniform sampling for a buried 4.2inch mortar (ID:473). The uniform sampling is using a fixed pre-defined sequence, where one transmitter is fired at any time and response were received at all twenty-five receivers. The choice of the transmitters are shown in red circles and their chronological indices are numbered in red. Uniform sampling used 18 out of 25 total transmitters to obtain a reliable and accurate feature estimate. (b) This plot shows the variation of feature estimation error as a function of sensing actions. Active selection and uniform selection are shown in red and blue, respectively. Note that active learning achieves the desired accuracy using only ten sensing action compared to eighteen actions taken by uniform sampling. (c) The adaptively selected transmitter activation sequence is shown in this plot, where the chronological indices are numbered in red.

the error in feature estimation is plotted as a function of the number of sensing actions. In absence of the “true” model parameters for the 4.2 inch mortar under observation, the model parameters estimated using all available Tx-Rx combinations (25 transmitters and 25 receivers, resulting in 625 Tx-Rx combinations) is treated as the “ground truth” and the model parameters estimated using Tx-Rx combinations chosen by the active and uniform sampling are compared against the ground truth to calculate the error in feature estimation. We have plotted the logarithm of the absolute feature estimation error as log-dispersion. It is important to note that active learning achieves the desired accuracy with much less sensing actions (10 vs 18) than uniform sampling. Figure 4(c) shows the adaptive choice of the transmitters as selected by our algorithm. Note that both approaches started with activating the same transmitter, but active learning quickly identifies the approximate location of the anomaly and takes sensing action from all orientation around the anomaly. This helps the algorithm to collect data that is more “relevant” for reliable estimation of target features.

Figure 5 presents an example of adaptive sensing where the target is not positioned at the center of the 5x5 grid. The buried anomaly is also a 4.2 inch mortar (ID:1006). Figure 5(a) displays the sequential choice of the transmitters for uniform sampling. Figure 5(b) compares the performance of the adaptive sensing scheme with the uniform sampling, measured in terms of feature estimation error. Active learning achieves the desired accuracy with six sensing actions compared to eighteen in uniform sampling. Figure 5(c) shows the adaptive choice of the transmitters as selected by our algorithm. It is interesting to observe that active learning quickly identifies the approximate location of the anomaly and takes sensing action around the anomaly, rather than following a fixed sequence.

SIG has also simulated a hand-held TEMTADS systems based on already available data on a 5x5 grid. In this approach, a 2x2 sensor block is allowed to maneuver on the existing 5x5 grid. This was particularly

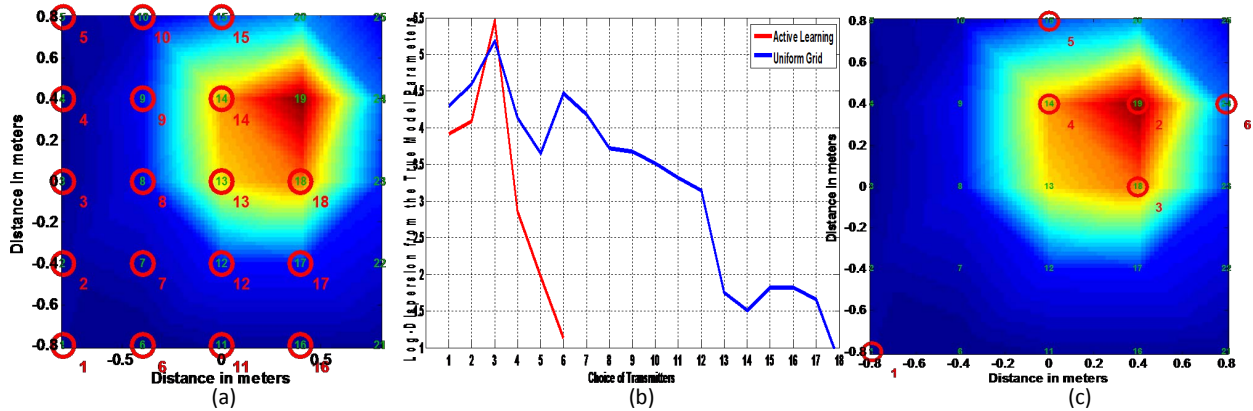


Fig. 5. (a) This plot shows the sequential choice transmitter’s activations for uniform sampling for a buried 4.2inch mortar (ID:1006). The choice of the transmitters are shown in red circles and their chronological indices are numbered in red. Uniform sampling used 18 out of 25 available transmitters to obtain an accurate estimate of anomaly features. (b) This plot shows the variation of feature estimation error as a function of sensing actions. Active selection and uniform selection are shown in red and blue, respectively. Active learning achieves the desired accuracy using only six sensing action compared to eighteen actions taken by uniform sampling. (c) The adaptively selected transmitter sequence is shown in this plot, where the chronological indices are numbered in red.

constraining since there exists only sixteen discrete locations at which a 2x2 sensor block could be positioned. However, SIG is aware that a hand-held version of the TEMTADS system (consisting of four transmitters and four receivers arranged in a 2x2 array) is currently being developed by Dr. Tom Bell and his colleagues at SAIC, funded by a separate SERDP program. The same group at SAIC is also developing a single transmitter-receiver coil system to be operated in hand-held configuration. It is supposed to collect data on a fixed grid placed above a buried anomaly. We think that the data collected by these systems would be helpful to validate our algorithm in the near future. At the current stage, SIG wanted to show the following analysis as a proof of concept given the small dataset that is already collected at Camp SLO. In the near future, SIG hopes to access data collected by the hand-held TEMTADS system and validate our approach on a more robust dataset.

In the hand-held environment, we assume that there will be a handheld system with four transmitters and four receivers arranged in a 2x2 array. Once a location is deemed “relevant” by the adaptive sensing algorithm, all four transmitters would be activated and anomaly responses would be recorded at all four receivers. Based on the collected data, SIG will estimate the model parameters and identify the next “best” location for the system to collect data. Since data are already collected on a 5x5 grid, SIG could only simulate the movement of the sensor system over the twenty-five point grid.

Figure 6 depicts the procedure that is followed to simulate a hand-held environment within the restriction of already collected data. Figure 6(a) shows the picture of a 4.2inch mortar (ID:1032) after it is excavated from the ground. Figure 6(b) shows the choice of the first 2x2 Tx-Rx block. Note that we already have data over a 5x5 grid, where the location of the transmitters are shown in green. The red square encompasses four adjacent transmitter locations (indexed as [1 2 6 7]), denoting that these transmitters and receivers were employed to collect data at this location. Figure 6(c) shows the choice of first two locations, where the second location involves transmitters [11 12 16 17]. Note that one location cannot be chosen more

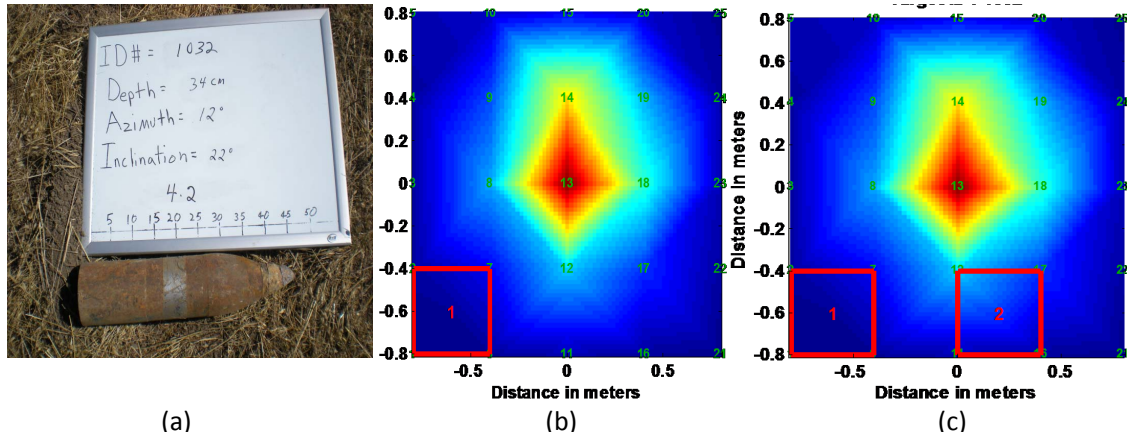


Fig. 6. (a) This image shows a 4.2inch mortar (ID:1032) after it has been excavated from the ground, (b) This image shows the selection of the first 2x2 transmitter-receiver block. The index of the individual transmitters are plotted in green (from 1 to 25). The 2x2 block chosen here corresponds to transmitters [1 2 6 7]. The choice is represented by a red square covering all the chosen transmitters. The background represents the monostatic response collected at all 25 receivers at first time gate. The 25 point responses are interpolated to produce a smooth image. (c) This plot shows the choice of first two 2x2 blocks, as decided by the adaptive sensing. Note that the second block is indexed as '2', marked in red, corresponds to transmitters [11 12 16 17].

than once, since we are restricted by the fact that data has already been collected.

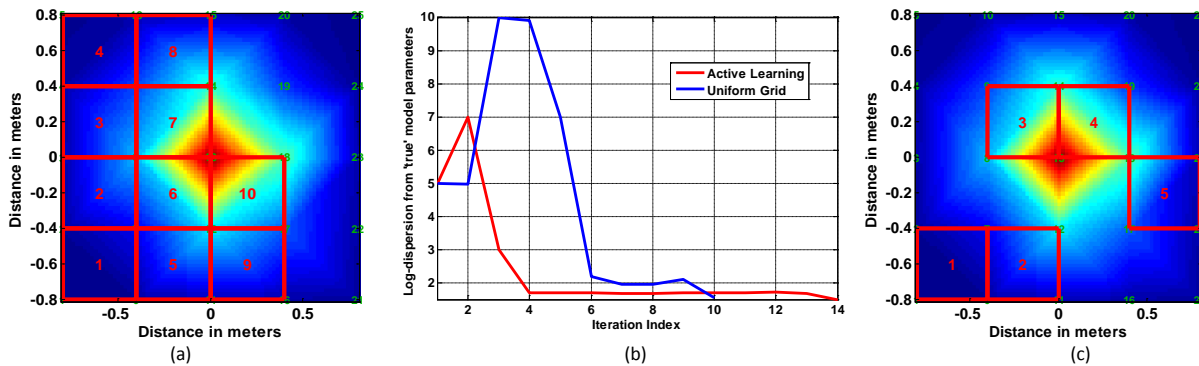


Fig. 7. (a) This plot shows the sequential choice of transmitter’s activations for uniform sampling for a buried 4.2inch mortar (ID:337). The uniform sampling is using a pre-defined sequence, where choice of transmitters in successive iterations are represented to bounding red squares with iteration index marked at the center of the square in red. (b) This plot shows the variation of feature estimation error as a function of sensing actions. Active selection and uniform selection performances are shown in red and blue, respectively. Note that active learning achieves the desired accuracy using only four sensing action compared to eight actions by uniform sampling. (c) The adaptively selected transmitter sequence is shown in this plot, where the chronological choices are marked in red.

Figure 7 compares the performance of the adaptive sensing approach with uniform sampling, in a 2x2 hand-held environment. Since we were restricted to operate over a fixed 5x5 grid, we allowed the 2x2 ‘simulated’ handheld to move only over these twenty-five grid points, and no multiple sensing at the same location were allowed. Figure 7(a) shows the choice of the uniform sampling, where the 2x2

was allowed to move in a N-S fashion. In contrast, Figure 7(c) shows the choice of the adaptive sensing, where the 2x2 block moves close to the true anomaly location and takes measurements around the object to reliably estimate the anomaly features with minimal sensing actions. It is worth noting that the active learning approach is a myopic approach that identifies the “next” best sensing action that would reduce the uncertainty in the model parameters. Hence this approach does not guarantee monotonic reduction in feature estimation error. The above example is a situation where the active learning approach has achieved a near-perfect estimation with only four sensing actions and subsequent actions do not achieve any further improvement. We have verified that all estimations where log-dispersion error is below two produce almost identical features.

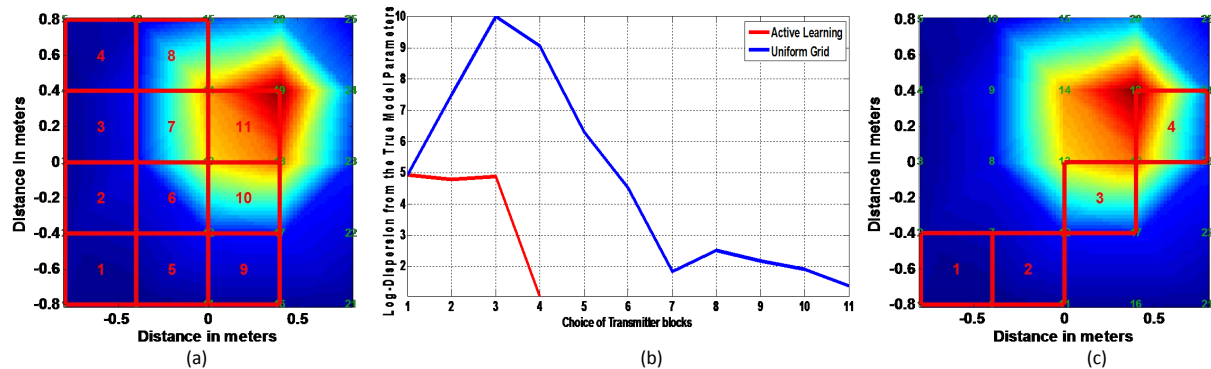


Fig. 8. (a) This plot shows the sequential choice of transmitter’s activations for uniform sampling for a buried 4.2inch mortar (ID:1006). (b) This plot shows the variation of feature estimation error as a function of sensing actions. Active selection and uniform selection are shown in red and blue, respectively. Note that active learning achieves the desired accuracy using only four sensing action compared to eleven actions taken by uniform sampling. (c) The adaptively selected transmitter sequence is shown in this plot, where the chronological indices are marked in red.

Figure 8 shows the efficacy of the adaptive sensing approach for another buried 4.2inch mortar (ID:1006), where the anomaly is not located at the center of the grid. It is interesting to observe that sensing locations, as guided by the adaptive learning scheme, gradually moves closer to the true target location and this helps the algorithm to obtain desired accuracy with only four sensing actions, compared to eleven sensing actions using uniform sampling. It is worth noting that Figure 8(a) on the left is an intrapolated image from twenty-five co-located Tx-Rx pairs. Signal strength corresponding to first measurement is relatively weak and noisy, but this gives us a starting set of model parameter estimates and guides us where to sample next.

Both approaches try to ascertain features of a buried anomaly using as few sensing actions as possible. Both approaches require no training data or a priori knowledge about an anomaly. It is a general approach applicable to any target model and any sensor system. First approach shows that a small subset of actively-selected transmitters are sufficient for reliable feature extraction, saving time and battery resources. The second approach shows that active-selection on a 2x2 sensor platform has capabilities similar to the 5x5 system, thereby increasing the mobility and usability of such a system on rugged terrains.

In addition to developing an adaptive sensing approach for the TEMTADS sensor (both hand-held and

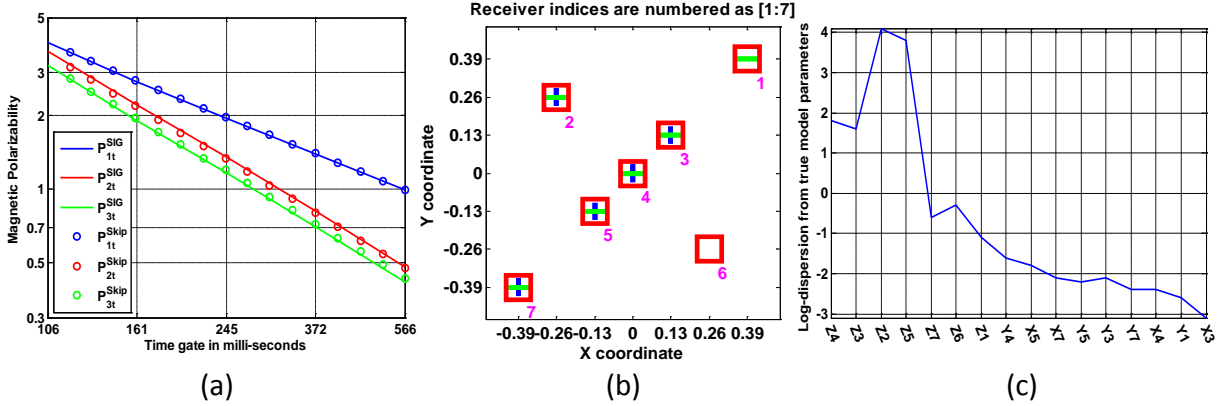


Fig. 9. (a) This plot shows the variation of the extracted magnetic polarizabilities along three principal directions as a function of response time. We obtain a strong magnetic moment (in blue) and two other near-similar moments (in red and green), as expected from a axisymmetric cylindrical 4.2inch mortar. The feature extractor used only actively-selected data. The circles represent the features obtained by Snyder Geoscience and they are nearly identical to the features extracted by our algorithm, (b) This schematic shows the Tx-Rx combinations that are deemed necessary by our active learning scheme. The indices of the receivers are numbered in magenta. A red square at receiver location ‘1’ represents that Transmitter Z was fired and response was collected by the receiver cube 1. Similarly, a green horizontal bar at location ‘7’ corresponds to activation of Ty and reception at receiver 7, and a blue vertical bar at location ‘2’ corresponds to activation of Tx and reception at receiver cube 2, (c) This plot shows the variation of feature estimation error as a function of sensing actions chosen. The Tx-Rx combinations are marked using two alphanumeric elements, where the first letter represents the transmitter chosen (*i.e.*, Z meaning Tz) and second element represents the receiver index (from 1 to 7).

towed-array configuration), SIG has also incorporated the active learning approach for the MetalMapper data collected at camp SLO. SIG has developed a reliable forward model in-house and verified that the in-house model corroborates with the results obtained by Skip Snyder of Snyder Geoscience. Following results show that both feature extraction approaches match very well. The data collection process employed by MetalMapper during the SLO study is both time and resource intensive. As mentioned in the previous section, a MetalMapper system consists of three orthogonal transmitter loops Tx, Ty, and Tz, positioned along X, Y and Z-direction. There are seven receivers placed on the horizontal plane, where each receiver location contains three-axis receiver coils placed in a cube. Hence, the system collects anomaly responses for twenty one Tx-Rx combinations, where each combination consists of data collected by all three co-located receivers at the corresponding receiver location. During the SLO demonstration study, the MetalMapper was deployed in cued mode, where each of the twenty-one Tx-Rx combinations were activated in a fixed sequence. The data collection and feature extraction phases were separate. In contrast, SIG has developed an adaptive learning approach, where one of the three transmitters would be activated at any time, and the anomaly response would be recorded at one of the seven receiver locations. Ideally, one would like to execute the active learning algorithm in real-time, where at each instance, one of the three transmitters is fired. We have simulated this scenario by allowing only one of the twenty-one transmitter-receiver pairs to be used at any time. The corresponding response is subjected to feature extraction, and the next “best” sensing action identified, *i.e.*, which transmitter-receiver combination needs to be activated next. The next “best” action is chosen in order to maximally reduce the uncertainty in the model parameters of the underlying anomaly.

Figure 9 shows the performance of the adaptive sensing approach for MetalMapper data collected for a 4.2inch mortar (MMID:1612). The figure on the left shows the final extraction of features using only actively selected data. These features are almost identical to the features extracted by Snyder Geoscience utilizing all available data. The figure in the middle shows the choice of the Tx-Rx combinations that are deemed “relevant” by our algorithm. A red square at receiver location ‘m’ represents that Transmitter Z was fired and response was collected by the receiver cube ‘m’. Similarly, a green horizontal bar at location ‘n’ corresponds to activation of transmitter Ty and reception at receiver ‘n’, and a blue vertical bar at location ‘p’ corresponds to activation of transmitter Tx and reception at receiver ‘p’. Figure 9(c) shows the variation in feature estimation error as a function of the sensing actions, as each sensing action choice is denoted as ‘[Ts rn]’, where Ts represents the transmitter oriented along $s \in \{x, y, z\}$, and rn represents the receiver cube at location ‘n’, with $n \in \{1, \dots, 7\}$.

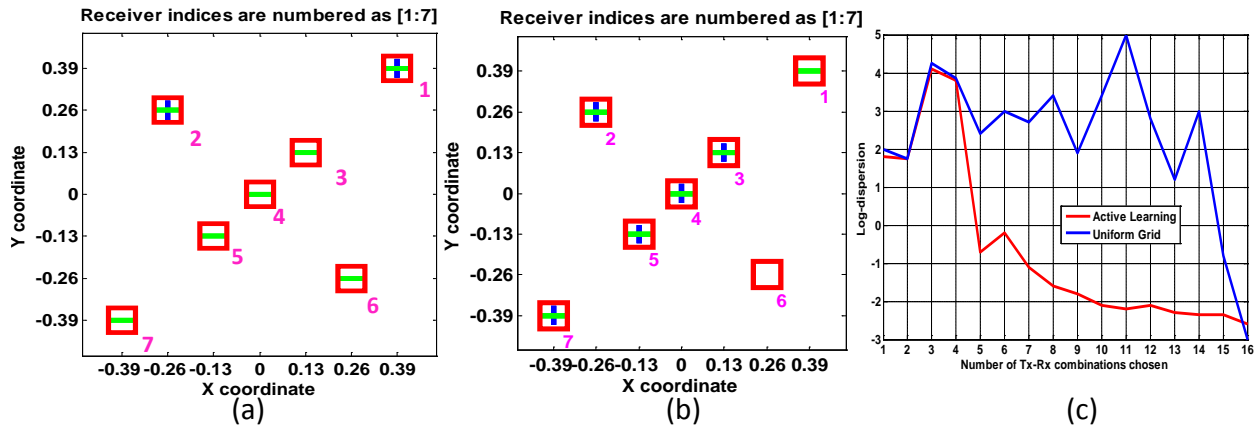


Fig. 10. (a) The schematic shows the Tx-Rx combinations chosen by the fixed sensor scheduling. SIG has assumed that Tz is activated first and receivers 1 to 7 are employed to collect the response. This is followed by activation of Ty and Tx respectively. The indices of the receivers are numbered in magenta. A red square at receiver location ‘m’ represents that Transmitter Z was fired and response was collected by the receiver cube m. Similarly, a green horizontal bar at location ‘n’ corresponds to activation of Ty and reception at receiver n, and a blue vertical bar at location ‘p’ corresponds to activation of Tx and reception at receiver p, (b) The schematic shows the Tx-Rx combinations chosen by adaptive sensor scheduling. (c) This plot compares the performance of active learning with fixed sensor scheduling by plotting the variation of feature estimation error as a function of number of sensing actions chosen.

Figure 10 compares the performance of the adaptive sensing approach for MetalMapper data collected for a 4.2inch mortar (MMID:1612) with the fixed sequence. Figure 10(a) and (b) correspond to the Tx-Rx combinations chosen by the fixed sequence and adaptive sequence, respectively. Figure 10(c) compares the performance, measured in terms of the feature estimation error. Note that adaptive sensing quickly reduces the estimation error with only eight sensing actions, whereas a fixed Tx-Rx combination needed sixteen sensing actions to obtain a similar performance.

Figure 11 shows the performance of the adaptive sensing scheme on MetalMapper data collected for a 2.36inch rocket (ID:33). The figure on the left shows the UXO after it has been excavated. The figure in the middle shows the choice of the Tx-Rx combinations by the adaptive sensing approach and the figure on the right compares the performance of adaptive sensing with fixed sensor scheduling. Active learning approach obtains reliable feature estimate using only seven sensing actions compared to sixteen in case

of fixed scheduling.

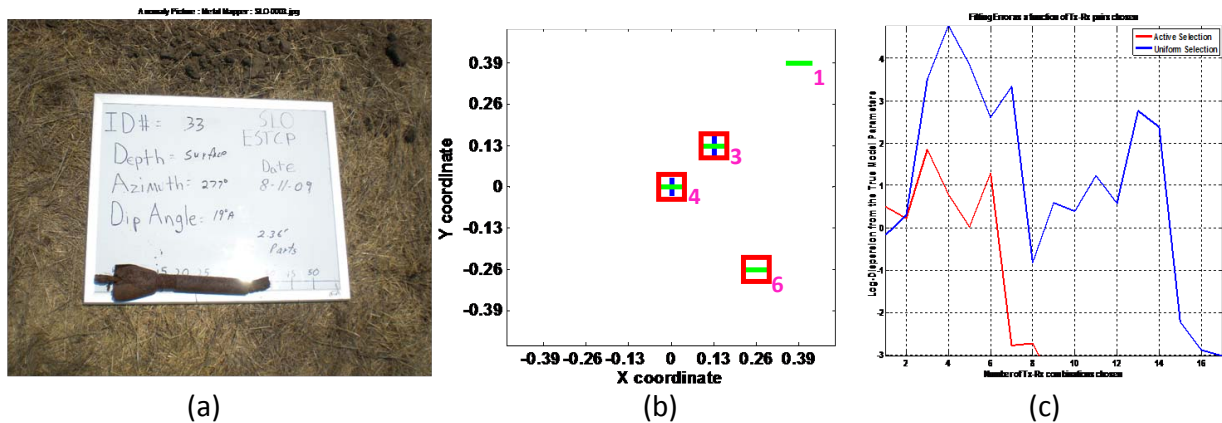


Fig. 11. (a) Photograph of a 2.36" rocket (ID:33) after it has been excavated from the ground, (b) This schematic shows the Tx-Rx combinations that are deemed 'relevant' by our algorithm, (c) This plot compares the performance of adaptive sensor scheduling with fixed scheduling, by displaying feature estimation error as a function of the number of sensing actions.

SIG has tried another adaptive selection approach for the MetalMapper, where the algorithm was only allowed to use a subset of the available receivers. Note that seven receivers are spread over the horizontal plane and we argued that if one could obtain similar performance by using only the inner five receivers, then the overall structure of the MetalMapper could be reduced, making it more lightweight and nimble, thereby increasing the speed of data collection. Figure 12 shows the performance of the adaptive sensing scheme on a restricted use of receivers. The figure on the left shows the Tx-Rx combinations deemed 'relevant' by the adaptive sensing approach, whereas the figure in the middle shows the choice using fixed sensor scheduling. The figure on the right compares their performances, measured in terms of feature estimation error. It is quite apparent that we could obtain a reliable and accurate feature estimation even if we restrict the choice of receivers. This allows us to infer that future reduction in MetalMapper hardware is possible without sacrificing quality of the collected data. We infer that coverage efficiency of the MetalMapper system in cued mode could be greatly enhanced (by saving time and battery power) if we integrate the active learning approach with data collection.

SIG had also proposed a Bayesian POMDP model for UXO classification using the BUD sensor as an additional task to be completed within the first year of the current program. Repeated discussion with the ESTCP program office and reviewers' feedback have motivated us revise our proposal to focus more on active learning-based sensor scheduling approaches for hand-held sensors. According to the reviewers, the BUD is designed to collect data at one location and is, therefore, less amenable to these methods. Therefore, SIG has modified the proposal and two approaches of active learning have been developed, one specifically for a hand-held system and the other for the towed-array configuration.

SIG plans to make all the relevant Matlab code available to all interested researchers. In addition, the authors plan to publish their work in a peer-reviewed journal in the near future. SIG has already written a white paper describing the framework and submitted it to the ESTCP program office in January 2010. The active learning algorithm needs to be incorporated in the sensor system in order to guide

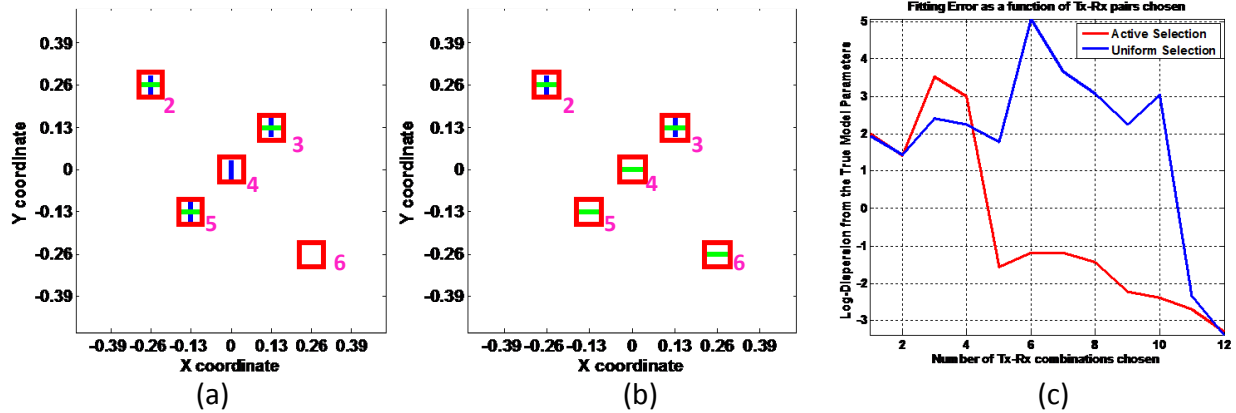


Fig. 12. (a) This schematic shows the choice of Tx-Rx combinations that are deemed relevant by the adaptive sensing scheme, (b) This schematic shows the choice of Tx-Rx combinations using fixed sensor scheduling, (c) This plot compares the performance of fixed and adaptive sensor scheduling, measured in terms of feature estimation error

the ground personnel to collect data selectively. Significant improvement in processing speed can be achieved by translating the code in C programming language. As proposed, SIG plans to validate the superior performance of active selection of data by implementing it on different sensor platforms (hand-held TEMTADS being developed by Tom Bell of SAIC) and different types of buried anomalies in the near future. In addition to the above sensor data, the active learning framework is also well-suited to a man-portable multi-axis system being developed at CRREL, under the guidance for Dr. Ben Barrowes and Dr. Kevin O’Neill. This project is also being funded by SERDP. SIG has communicated with Dr. Barrowes and has learnt that the MPV system is currently being redesigned and will be ready to collect data during this summer. SIG would like access the data from this sensor as they become available.

V. CONCLUSIONS AND FUTURE WORK

SIG has developed an information theoretic framework for adaptively selecting where and how to collect data in order to ascertain the geophysical parameters of a buried anomaly with minimal number of sensing actions. We have developed two adaptive approaches for the next-generation TEMTADS sensor. The first approach activates one transmitter at a time while collecting response at all twenty five receivers. We have shown that one can perform accurate and reliable feature inversion with much less sensing actions using active learning than uniform sampling. In the second approach, we have simulated a hand-held environment where a 2x2 block of TEMTADS sensor system working under the guidance of adaptive sensing methodology was shown to perform similar to the big and bulky towed-array system that was deployed in the SLO demonstration study. This analysis suggests that a hand-held TEMTADS sensor will be able to retain its UXO discrimination capability while being light, nimble and easily maneuverable. We have also incorporated the active learning approach for the MetalMapper sensor. Our analysis shows that one can save both data collection time and power consumption by selectively collecting data for model parameter inversion. Our simulation also suggests that a more compact MetalMapper sensor employing only five inner receivers would be sufficient for discriminating UXO from clutter.

REFERENCES

- [1] Y. Zhang, X. Liao, and L. Carin, "Detection of buried targets via active selection of labeled data: application to sensing subsurface uxo," *IEEE Transactions on Geoscience and Remote Sensing*, vol. 42, pp. 2535–2543, 2004.
- [2] B. Delaney and D. Etter, *Report of the Defense Science Board Task Force on Unexploded Ordnance*, <http://www.acq.osd.mil/dsb/reports/uxo.pdf>, 2003.
- [3] H. Nelson and J. McDonald, "Multisensor towed array detection system for uxo detection," *IEEE Transactions on Geoscience and Remote Sensing*, vol. 39, no. 6, pp. 1139 – 1145, June 2001.
- [4] Y. Zhang, H. Y. L. Collins, C. Baum, and L. Carin, "Sensing of unexploded ordnance with magnetometer and induction data: Theory and signal processing," *IEEE Transactions on Geoscience and Remote Sensing*, vol. 41, pp. 1005–1015, May 2003.
- [5] X. Liao and L. Carin, "Application of the theory of optimal experiments to adaptive electromagnetic-induction sensing of buried targets," *IEEE Transactions on Pattern Analysis and Machine Intelligence*, vol. 26, no. 8, pp. 961–972, 2004.
- [6] M. H. DeGroot, *Probability and statistics (2nd Ed.)*. Addison-Wesley Publishing Company, 1986.
- [7] V. V. Fedorov, *Theory of Optimal Experiments*. Academic Press.
- [8] T. Cover and J. Thomas, *Elements of information theory*. New York, NY, USA: Wiley-Interscience, 1991.
- [9] T. Bell, SAIC, H. Nelson, NRL, D. George, G&G, D. Steinhurst, Nova Research Inc., J. Kingdon, SAIC, and D. Keiswetter, SAIC, "EMI Array for Cued UXO Discrimination," 2008, submitted for publication.